Korean J. Chem. Eng., 38(8), 1703-1714 (2021)
DOI: 10.1007/s11814-019-0462-0

pISSN: 0256-1115
eISSN: 1975-7220

3-D modeling of proton exchange fuel cell cathode with a novel random generation of gas diffusion porous layer

Reza Bahoosh*,†, Moosa Jafari, and Seyed Saied Bahrainian***

*A Faculty Member of Mechanical Department of Shahid Chamran University of Ahvaz, Ahvaz, Iran
**Ph.D. Student of Mechanical Department of Shahid Chamran University of Ahvaz, Ahvaz, Iran
(*Received 22 June 2019 • Revised 20 August 2019 • Accepted 10 December 2019*)

Abstract−A 3D model for a section of cathode fuel cell comprised of a bipolar plate, a gas diffusion layer (GDL) and a catalyst layer was simulated. The diameter of the carbon fiber GDL is assumed to be the same; moreover, a new and simple method is introduced for the reconstruction of this layer numerically. This method gives the ability to model the heterogeneous and anisotropic structure of the GDL; furthermore, it allows easy implementation and provides realistic results with consideration of the lack of overlap between carbon fibers. The lattice Boltzmann method (LBM) was employed to simulate the flow and the electrochemical reaction. The impacts of changes in the activation potential and the GDL carbon fiber diameter on oxygen species and water vapor, as well as the electric current density distribution over the catalyst layer, were studied. The results showed that at higher values o f the activation potential, the concentration of oxygen near the catalyst layer was lower. The current density over the catalyst layer also increased by increasing the activation potential; on the other hand, the mole fraction of water vapor in the cathode increased with the increase in the flow of gas products. Consequently, results indicated that the variation in the GDL carbon fiber diameter affects the distribution of reactants.

Keywords: 3-D Modeling, Random Generation, Gas Diffusion Layer, Proton Exchange Fuel Cell, GDL

INTRODUCTION

The ever increasing demand for energy and the overwhelming environmental complications compel the use of renewable and green energy sources. Fuel cells, in particular, polymer electrolyte membrane (PEM), show great potential in this regard [1-4]. Fuel cells have become popular with simple principles of operation; in contrast, the production energy has a high price yet. The last two decades of study focused on fuel cell were successful in reducing the electricity production costs; on the other hand, achieving the optimal requires further research [5,6]. The evolution of fuel cell research in a holistic approach as modeling a complete fuel cell has changed to the partial approach as modeling of components of the fuel cell. Meanwhile, accounting for an extensive body of research of the gas diffusion layer (GDL) [7-13] is a noteworthy component. Because of its functions, which include directing the gas reactants towards the catalyst powder, conducting the electrical current to the collector plate, exhausting the generated heat outside the cell and managing the produced water in the PEM fuel cell [14-16], the GDL layer is required to be modeled with excellent accuracy for the purpose that studies the impact of different parameters on cell performance is considered. Considering the role of the GDL in thermal and electrical conduction, as well as retaining the catalyst, it is required to offer excellent thermal conductivity, electrical conductivity, and mechanical strength; for that reason, the GDL is often fabricated of [non-woven] carbon paper, or [woven] carbon cloth. GDLs made of carbon paper are thinner with less flexibility and are widely used because of high permeability for gases and high electrical conductivity. As a result of lower cost and easier creation of a microporous layer or a catalyst layer, fuel cell manufacturers often use carbon paper [17,18].

To produce carbon paper, carbon fibers are laid in layers and joined by an adhesive. This method of fabrication yields carbon paper with a non-uniform distribution of carbon fibers and providing a non-homogeneous and anisotropic porous medium. The non-uniformity of the pores in the GDL has a considerable impact on the transmission parameters of the porous layer, making it irrelevant to average the parameters without modeling the flow. Oversimplification in the assumptions for modeling the GDL such as ignoring the layer structure allows error formation in modeling results [19,20]. To create a realistic three-dimensional GDL structure, researchers use 3D scanning [21,22], combining 2D images [22,23] and random generation [24-27]. Meanwhile, thanks to its facileness, researchers often employ the random generation method. Random models are created by randomly recurring solid parts in a space. Considering the cylindrical shape of constituent carbon fibers of GDL, the solid particles in the generated porous medium must be cylindrical. With every fiber added, the empty space is divided into smaller pores. The random placement of cylindrical particles in a space can be either softcore or hardcore [28].

In the softcore approach, the constituent solid particles of the porous medium may overlap and their production continues until the desired porosity is attained [29,30]. Because of its simplicity, this random GDL production method is often employed. Assuming coplanar carbon fibers of the same thickness, Chen et al. [31] presented a 3D GDL model. In the following, they obtained a 2D cross-

†To whom correspondence should be addressed.
E-mail: bahoosh@scu.ac.ir

section of the GDL and evaluated the flow of reactants at the cathode of a fuel cell. Their GDL structure allowed the intersection between the fibers containing a uniform random distribution direction. By use of the model proposed by Schules [32], Hao, and Cheng [33] reconstructed the GDL structure. Assuming the diameter of carbon fibers is uniform and the possibility of overlap between carbon fibers, they studied the permeability and tortuosity of this porous medium. Considering the layered structure of GDL, Wang et al. [34] assumed it was composed of several independent layers, where carbon fibers from different layers were only in contact with each other. Even though many researchers consider the softcore approach to reconstruct the fibrous porous medium, the notion of intersecting carbon fibers is not physically possible; finally, hardcore approaches were proposed [35-38]. Although hardcore models are more realistic, they are also more difficult to implement in comparison with softcore models. After reconstructing the GDL to study the emission of reactants and model the electrochemical reaction, the flow equations inside the cathode must be solved. As it was mentioned earlier, the porous structure of the electrode is non-homogeneous and complex; hence, simulating with classical computational fluid dynamics (CFD) will prove to be difficult. Consequently, the lattice Boltzmann method, which has the intrinsic capability for solving the flow in complex media, was employed [25,31,39-42].

In this study, a 3D model of the fuel cell cathode is presented to study the flow and evaluate the distribution of the electric current density over the catalyst layer. Because of the difficulties of implementing the proposed hardcore approach, assuming the GDL is composed of independent layers [34], a novel and simple approach to the layer reconstruction is applied. Cylindrical carbon fibers of identical thicknesses are created randomly in every layer. These cylindrical particles are created in parallel to the horizon and random orientation with no overlap. Finally, the flow and the electrochemical reaction are simulated over a domain extending across a portion of the bipolar plate, the GDL, and the catalyst layer by the lattice Boltzmann method. According to the references cited in the text and other reviews of the current study authors, no such combination has been used to model the gas diffusion layer. In summary, this paper has attempted without using the fiber overlap possibility assumption, contrary to references [32-34,42], and unlike conventional hardcore approaches, ref. [35-38], to provide a simple and efficient method.

LATTICE BOLTZMANN METHOD

The LBM employed in the present study is based on the model presented by Bhatnagar, Gross, and Krook [43]. The discrete governing equation is as follows:

$$f_i(r+c_i\Delta t\cdot t+\Delta t)-f_i(r\cdot t)=-\frac{1}{\tau}(f_i(r\cdot t)-f_i^{eq}(r\cdot t)) \tag{1}$$

where f_i and f_i^{eq} are the distribution function and the equilibrium distribution function respectively. i represents the direction in the selected D_nQ_m arrangement, where n indicates the dimensions of the problem and m is the number of pathways at each node. 3 dimensions and 19 pathways at each node (Fig. 1) are considered in the present study. Δt and τ represent the time-step and the relaxation time, respectively. According to the following equation, the relaxation time τ depends on fluid viscosity:

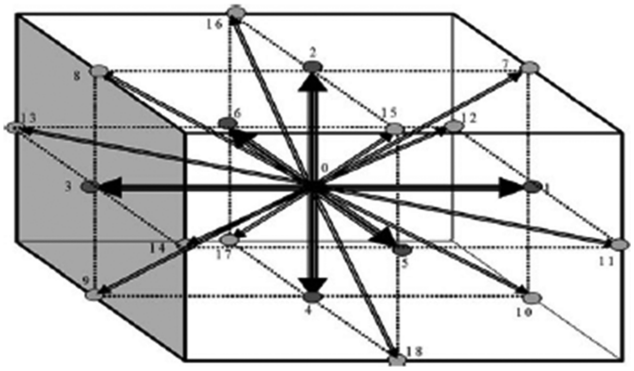

Fig. 1. D_3Q_{19} arrangement.

$$\upsilon=\frac{\Delta x^2}{3\Delta t}\left(\frac{1}{\tau}-0.5\right) \tag{2}$$

where in Eq. (1), c_i represents the velocity in different pathways and is defined as follows for the D_3Q_{19} arrangement:

$$c_i=\begin{cases}(0.0.0) & i=0\\ (\pm1.0.0).(0.\pm1.0).(0.0.\pm1) & i=1:6\\ (\pm1.\pm1.0).(\pm1.0.\pm1).(0.\pm1.\pm1) & i=7:18\end{cases} \tag{3}$$

The equilibrium distribution function f_i^{eq} is defined as follows:

$$f_i^{eq}=w_i f\left[1+\frac{c_i\cdot u}{(c_s)^2}+\frac{(c_i\cdot u)^2}{2(c_s)^4}-\frac{u\cdot u}{2(c_s)^2}\right] \tag{4}$$

where w_i is the weight factor (w_0=12/36, $w_{i=1:6}$=2/36, $w_{i=7:18}$=1/36) in the D_3Q_{19} arrangement. c_s is the speed of sound in the fluid and is expressed as $c_s=c/\sqrt{3}$ where $c=\Delta x/\Delta t$. The density ρ and velocity u are calculated by the following relationships in the LBM:

$$\rho=\sum_i f_i \tag{5}$$

$$\rho u=\sum_i f_i c_i \tag{6}$$

Although Eq. (1) is the main equation in the LBM, the developed LBMs must be utilized for the multi-species flow of air and water vapor inside the GDL. Two approaches, active and inactive, have been proposed in this regard [44]. In the inactive approach, the single-phase multi-species flow equation is only used for the dominant species in the gas blend, whereas, in the active one, streaming and contact are used for each species separately. In the second method, inspired by the model presented by Shan and Chen [45], the velocity of every species in Eq. (1) is replaced with a composition velocity $\vec{u}_{comp}$:

$$\vec{u}_{comp}=\frac{\Sigma_n\frac{1}{\tau_n}\Sigma_i f_n^i\vec{C}_i}{\Sigma_n\frac{1}{\tau_n}} \tag{7}$$

Applying boundary conditions in the LBM requires the unknown

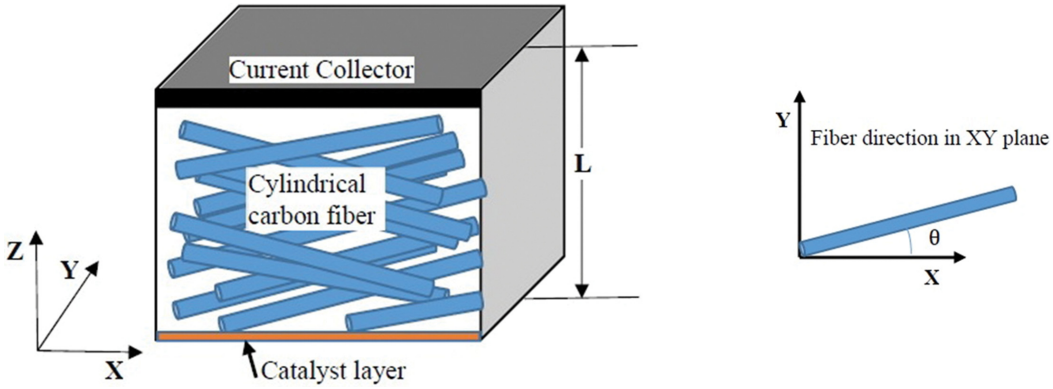

Fig. 2. Cubic part of PEM cathode.

distribution functions to be calculated at each boundary according to the physical conditions. An important feature of the LBM is its capacity for modeling boundaries of complex geometries by using the bounce-back boundary condition. More details on the LBM and the application of different boundary conditions can be found in the literature [46,47].

METHODOLOGY

1. 3D Cathode Model

The PEM fuel cell is composed of a GDL, a catalyst layer, a bipolar plate at the cathode and anode sides as well as a polymer membrane. The oxygen reduction (water production) in reaction takes place at the cathode, which is often studied because of the fact that water management in the cell is significant. Fig. 2 presents a schematic view of the problem, illustrating a portion of the current collector, the GDL and the catalyst layer. The dry airflow, comprising 21% oxygen and 79% nitrogen enters the system from the left boundary. Air is passing through the GDL by diffusion and convection; the oxygen in the air reaches the catalyst layer at the cathode where it reacts with the hydrogen generated at the anode. Water is produced according to the following equation by oxygen reduction at the cathode:

$$4H^+ + O_2 + 2e^- \rightarrow 2H_2O \tag{8}$$

Through an electrochemical reaction over the surface of the catalyst layer and the production of water vapor, the gas mixture leaves the cell from the left surface. The gas mixture was assumed to behave like an ideal gas. The catalyst layer is located at Z=0 level, and the electrochemical reaction takes place over it. Oxygen reduction (Eq. (8)) is quite slow and must take place adjacent to the catalyst. Platinum is an excellent catalyst for this reaction but its high price dramatically increases the electricity production costs. Accordingly, through novel fabrication methods and by increasing the catalyst active surface area, researchers have managed to reduce the Pt loading at the cathode. Hence, the catalyst layer is composed of Pt nanoparticles on a carbon-fiber bed and membrane. That being said, many previous modeling [31,44,48] attempts assumed a very thin catalyst layer, which was taken into account as a boundary condition. The method proposed by Kamali et al. [49] was employed to apply the reaction boundary condition in the current LBM. By modifying the bounce-back boundary condition and according to the chemical reaction rate on the catalyst surface, a percentage of oxygen molecules colliding this layer react and are converted to water molecules, while the rest remains unchanged and enter the solution domain. Furthermore, the reaction boundary conditions in the LBM can be applied by calculating this fraction. The reaction rate constant is proportional to the physical reaction rate constant as follows [49]:

$$K_{sr}^{LB} = \left(\frac{6K_{sr}\Delta t}{\Delta x}\right) \Big/ \left(1 + \frac{K_{sr}\Delta x}{2D}\right) \tag{9}$$

where K_{sr} is the reaction rate constant, Δt, Δx, D and are the time step, the discrete lattice and the diffusivity of oxygen in the blend, respectively. In oxygen reduction (Eq. (8)), the surface reaction constant K_{sr} depends on the electric current density j, generated during the reaction:

$$K_{sr} = \frac{j}{4F\rho_{O_2}} \tag{10}$$

where F is the Faraday constant and ρ_{O_2} represents the density of oxygen over the cathode catalyst surface. The electric current density over the catalyst layer can be calculated by the Butler-Volmer equation [50] as follows:

$$j = a^{roughness} j^{ref} \left(\frac{\rho^O}{\rho^{O.ref}}\right) \left[\exp\left(\frac{\alpha_f F \eta}{R_u T}\right) - \exp\left(-\frac{\alpha_r F \eta}{R_u T}\right)\right] \tag{11}$$

In Eq. (11), j, $a^{roughness}$ and j^{ref} represent the electric current density, the roughness coefficient (the ratio of the actual catalyst surface area to its apparent area) and the reference current density, respectively. ρ^O. α_f and α_r are the oxygen reference density and the transport coefficients in the forward and backward reactions, respectively. According to Eqs. (10) and (11), we have:

$$K_{sr} = \frac{a^{roughness} j^{ref}}{4F} \left(\frac{1}{\rho^{O.ref}}\right) \left[\exp\left(\frac{\alpha_f F \eta}{R_u T}\right) - \exp\left(-\frac{\alpha_r F \eta}{R_u T}\right)\right] \tag{12}$$

2. Gas Diffusion Layer Reconstruction

The GDL plays a critical role in the function of a fuel cell; therefore, modeling its structure allows improving GDL performance. Furthermore, to model the gas flow and the electrochemical reaction in the cell, it is necessary to apply the governing equations to the solution domain of the cathode structure. If modeling of GDL

structures is more accurate, the results of modeling will be closer to reality.

In carbon paper fabrication, carbon fibers are randomly placed within the GDL and the structure of this layer is completely non-homogeneous and anisotropic; images of the GDL microstructure are required to obtain the pore structure and the fiber diameter distribution. However, given the difficulty arising from modeling complexity and the cost of the method, many researchers rely on random generation to reconstruct the GDL [31,44,48]. Since the carbon fibers are solid and have relatively high strength, the hypothesis of overlap between carbon fibers and the use of methods for producing a softcore structure does not seem to be logical. The gas diffusion layer is made of carbon fiber layers; therefore, it can be assumed that all these separated layers have porosities equal to the total porosity of the GDL.

Furthermore, considering the fabrication process and the microstructural images, it is assumed that the carbon fibers in the layer are cylindrical without curvature, with identical diameters and also horizontal [34]. By considering the discussed assumptions, the reconstruction of the GDL structure is explained in the following.

3. Specifying Dimensions of Model, Porosity and the Carbon Fiber Diameter

The real dimensions of fuel cell cathode assuming a one-micrometer distance between the lattice nodes are 1,200×180×180 approximately; only a portion of the domain is simulated. Owing to the fact that limitations of the computer hardware exist, the current collector, the catalyst layer and the GDL, were taken into account (Fig. 2); moreover, 101×101×101 lattice was used in this study. The porous medium was generated by MATLAB code, which allows input of the porosity and the diameter of carbon fiber to be applied for a parametric study.

4. Generating a Random Porous Medium at the GDL

As mentioned, the GDL produced from carbon paper is composed of separate thin layers of carbon fiber that are joined by an adhesive [34]; assuming carbon fibers with no curvature, it is enough to create straight horizontal lines on the X-Y plane through random generation (Fig. 2). For the creation of a random straight line, one point and a unit vector are required. To create a random point, it will suffice to use the Rand function in MATLAB. First, the selected point must be located on the solution domain and second, it should be checked in such a way adjacent fibers do not overlap. Since carbon fibers are assumed parallel to the X-Y axis, to generate a random unit vector, it is only necessary to create an angle θ in Fig. 2 randomly.

To make possible the investigation of the effects of carbon fiber on the performance of a fuel cell, the Normrnd (mu, sd) function was utilized to randomly generate an angle. Where mu represents the average randomly generated angle and sd is the standard deviation of the created numbers. To produce the cylinder, it is necessary to identify nodes of the solution domain that are located less than the radius of carbon fiber of the line and to be placed as solid porous media. For this purpose, the following equation is adopted:

$$h = \left|\overrightarrow{PX_2} \times \overrightarrow{PX_1}\right| / (|X_2 - X_1|) \tag{13}$$

where X_1 and X_2 are two points on the produced line and P is an arbitrary point in space; therefore, h is the distance between the point and the line (Fig. 3). In the hardcore method, randomly generated structures, the cylinders are not allowed to share nodes; this is not challenging when creating the first fiber in each layer. However, for the production of new fibers within this layer, it is necessary to produce random lines that do not collide with previously produced lines (fibers).

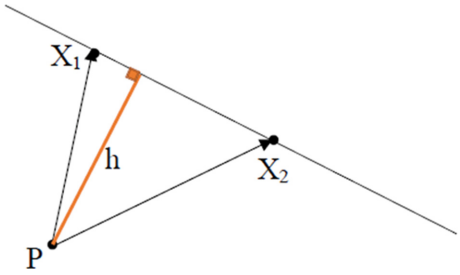

Fig. 3. Point distance from the created line.

Given that if two cylinders collide, the distance between their axes is less than the diameter of the carbon fiber. In the production of new fiber, the conductor's point (P) and axis must be in such a way that they are not exposed to other carbon fibers. For this, the points of the domain, which are in the early stages as part of carbon fiber and solid, must be at least equal to a fiber diameter from the new random line. Hence, for the production of random lines in each layer, the following condition must be checked and, if the line condition is satisfied, it can be considered as the axis of creating a new fiber [51]:

$$d_1 = |ax_0 + by_0 + c| / \sqrt{a^2 + b^2} \geq D \tag{14}$$

where ax+by+c=0 is the equation of a new generated line and (x_0. y_0) is a point on the previously produced centerline. The random generation of lines in the layer continues until the required porosity is attained. After the generation of porosity is completed in one layer, the creating porous structure is continued in other layers. The flowchart of the carbon fiber structure generation of the GDL is depicted in Fig. 4.

5. Boundary Conditions

The dry air flows in the x-direction enter the cathode (Fig. 2). Constant pressure boundary conditions with a small pressure difference were applied to the model to establish gas flow [52]; the method proposed by Zou and He [53] was utilized. As a result, the unknown functions f_1, f_{12}, f_7, f_{11} and f_{10} are obtained on the X=0 plane whereas f_2, f_9, f_8, f_{13}; and f_{14} are calculated on the X=L plane based on the known distribution functions in the streaming process as follows:

$$\begin{aligned}
&u = 1 - (f_2 + f_4 + f_5 + f_6 + f_{15} + f_{16} + f_{17} + f_{18} + 2(f_3 + f_8 + f_9 + f_{13} + f_{14}))/\rho \\
&f_1 = f_3 + \rho u/3 \\
&f_7 = f_9 + \rho u/6 - (f_2 + f_{16} + f_{15} - (f_4 + f_{17} + f_{18}))/2 \qquad X=0 \\
&f_{10} = f_8 + \rho u/6 + (f_2 + f_{16} + f_{15} - (f_4 + f_{17} + f_1))/2 \\
&f_{11} = f_{13} - \rho u/6 + (f_1 + f_7 + f_{10} - (f_3 + f_8 + f_9))/2 \\
&f_{12} = f_{14} + \rho u/2 - (f_1 + f_7 + f_{10} - (f_3 + f_8 + f_9))/2 \qquad (15) \\
&u = -1 + (f_2 + f_4 + f_5 + f_6 + f_{15} + f_{16} + f_{17} + f_{18} + 2(f_1 + f_7 + f_{10} + f_{11} + f_{12}))/\rho \\
&f_2 = f_2 - \rho u/3 \\
&f_9 = f_7 - \rho u/6 + (f_2 + f_{16} + f_{15} - (f_4 + f_{17} + f_{18}))/2 \qquad X=L
\end{aligned}$$

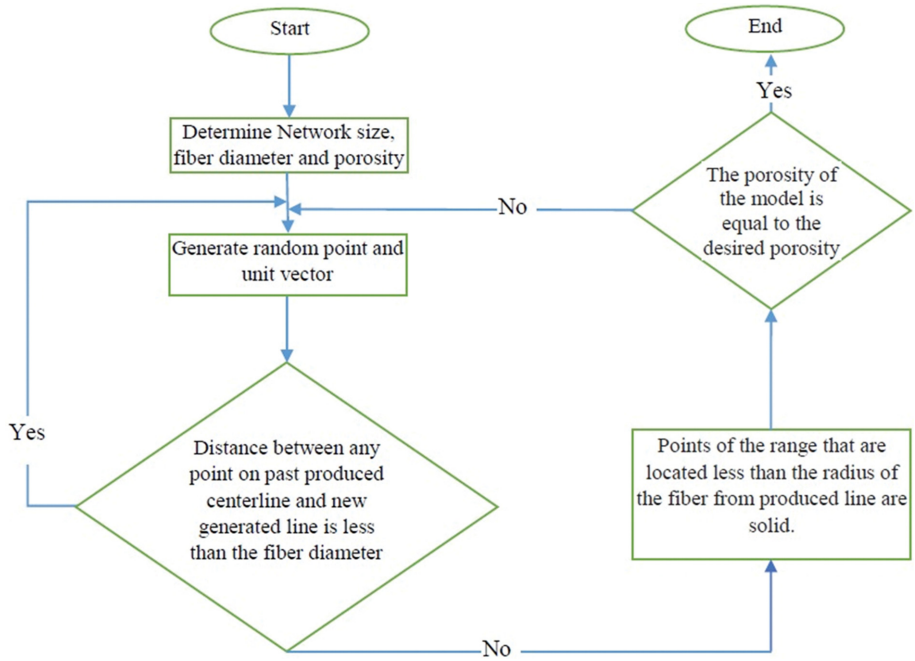

Fig. 4. GDL structure generation flowchart.

$$f_8=f_{10}-\rho u/6+(f_2+f_{16}+f_{15}-(f_4+f_{17}+f_{18}))/2$$
$$f_{13}=f_{11}+\rho u/6-(f_1+f_7+f_{10}-(f_3+f_8+f_9))/2$$
$$f_{14}=f_{12}-\rho u/2+(f_1+f_7+f_{10}-(f_3+f_8+f_9))/2$$

The above relations (Eq. (15)) must be solved for each species separately and the mole fractions must be specified to calculate partial pressures. It is easy to calculate the partial pressure on X=0 because of the absence of water vapor and the determination of oxygen and nitrogen mole fractions in the gas mixture.

However, considering that the composition of the gas blend is not known at the outlet (X=L plane), it is not possible to calculate the partial pressures of oxygen, nitrogen, and water vapor. To solve this problem, it is assumed that the density of each species over the X=L plane is equal to its density over the X=L−1 plane [44].

The catalyst layer, which serves as an impermeable reaction boundary, is located at the Z=0 boundary and is assumed to have a negligible thickness. The reaction boundary condition proposed by Kamali et al. [49] is adopted as follows for obtaining the equilibrium distribution functions:

$$\begin{aligned}
f_2^W &= K_s^{LB}\times f_4^{O_2}+f_4^W & f_2^{O_2} &= (1-K_s^{LB})\times f_4^{O_2}\\
f_{16}^W &= K_s^{LB}\times f_{18}^{O_2}+f_{18}^W & f_{16}^{O_2} &= (1-K_s^{LB})\times f_{18}^{O_2}\\
f_{15}^W &= K_s^{LB}\times f_{17}^{O_2}+f_{17}^W & f_{15}^{O_2} &= (1-K_s^{LB})\times f_{17}^{O_2}\\
f_7^W &= K_s^{LB}\times f_9^{O_2}+f_9^W & f_7^{O_2} &= (1-K_s^{LB})\times f_9^{O_2}\\
f_8^W &= K_s^{LB}\times f_{10}^{O_2}+f_{10}^W & f_8^{O_2} &= (1-K_s^{LB})\times f_{10}^{O_2}
\end{aligned} \tag{16}$$

The boundary conditions of Eq. (7) are only applicable to the species taking part in the electrochemical reaction (oxygen and water vapor), whereas for nitrogen species, the bounce-back boundary condition is established at the Z=0 boundary.

The $Z=L_z$ plane lies over the current collector solid and the bounce-back boundary condition, which represents the non-slip boundary condition in a physical space, is utilized at this boundary as well as the carbon fiber boundaries inside the GDL. The symmetry boundary condition was also assumed over Y=0 and Y=L planes.

RESULTS

The lattice Boltzmann method (LBM) was employed to investigate the flow, the distribution of species and the electrochemical reaction in a section of a fuel cell cathode consisting of the bipolar plate, the GDL, and the catalyst layer (Fig. 2). The GDL, which accounts for the centerpiece of the model, is formed with the random generation of cylinders of equal diameters in a manner that prevents any overlap between them. MATLAB coding was performed to create the porous media of the gas diffusion layer and solve the LB equations. Before simulating the flow inside the model developed by the proposed method, the GDL was evaluated according to the most important parameters of the porous medium, including permeability and tortuosity.

1. Validation

An important parameter in porous media is the capability to flow pass through it, represented by permeability (K). According to the Darcy equation for a continuous, single-phase flow with low Reynolds and constant fluid properties, the permeability is defined with the pressure gradient as follows [54]:

$$K=-\frac{\mu\langle u\rangle}{\Delta P} \tag{17}$$

In Eq. (17), $\langle u\rangle$, μ, ΔP are the space-averaged velocity, the dynamic viscosity and the pressure gradient applied to a sample volume, respectively. The permeability changes with the shape and position of the pores. The Kozeny-Carman equation is commonly used to estimate the permeability of a porous medium [55]:

$$K = \frac{\varepsilon^3}{180(1-\varepsilon)} d^2 \quad (18)$$

In the Kozeny-Carman, ε represents the porosity, and d is the mean diameter of the solid particles in a porous medium. Kaponen et al. measured permeability in a 3D porous medium with a randomly-distributed fiber texture [56]. They proposed the following equation to measure permeability as follows:

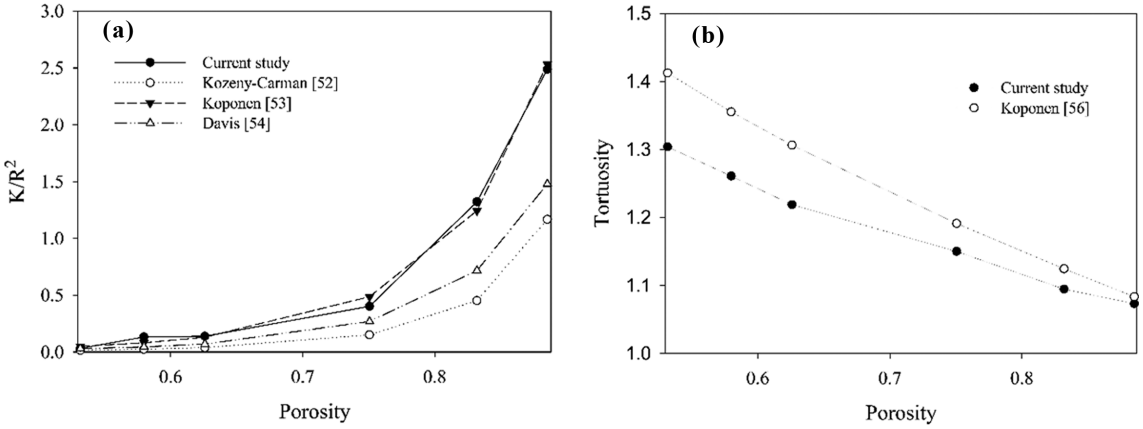

Fig. 5. Predicted permeability and tortuosity of the proposed model.

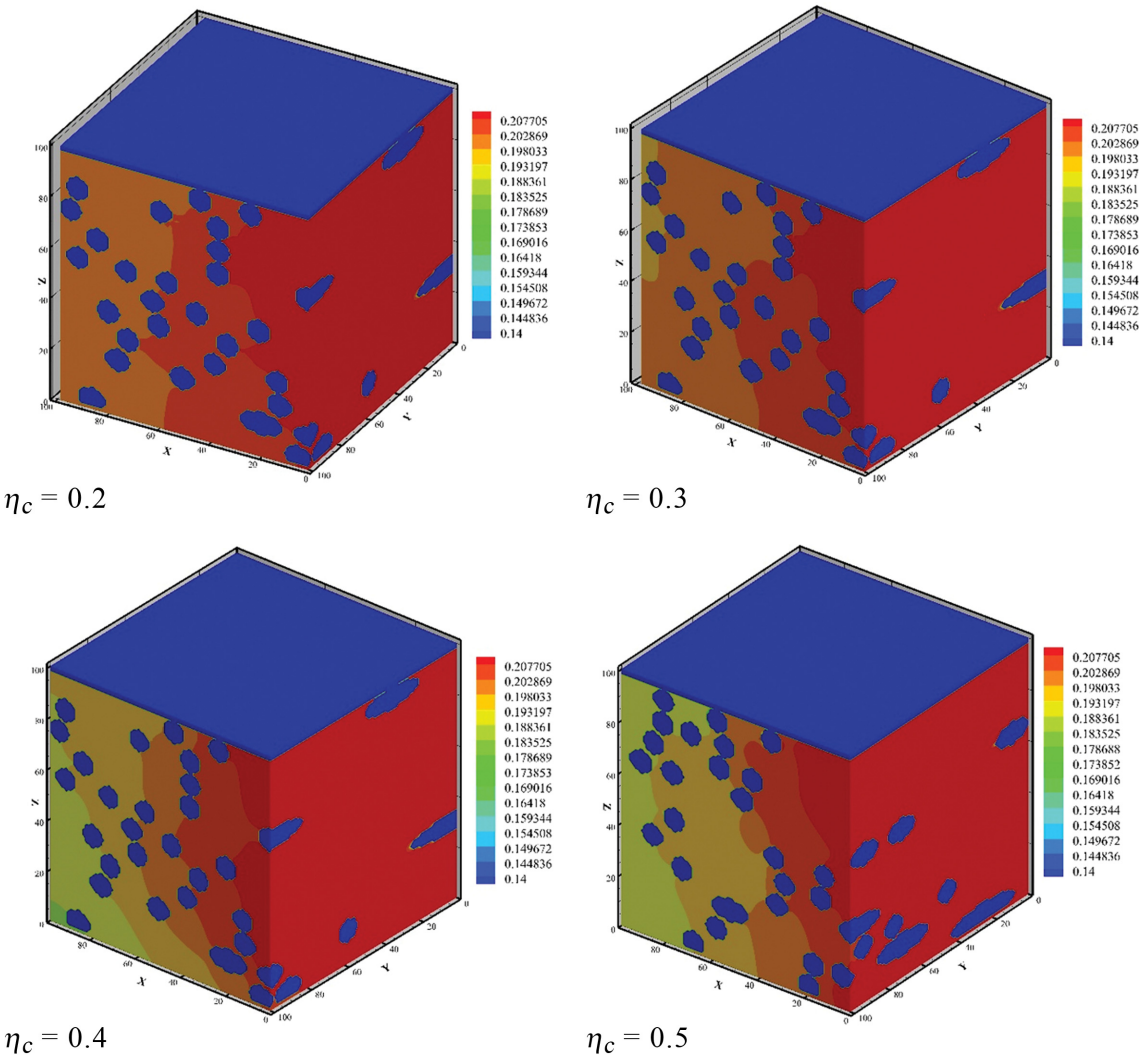

Fig. 6. Distribution of oxygen mole fraction.

$$K=\frac{d^2}{4}A(e^{B(1-\varepsilon)}-1)^{-1} \quad (19)$$

In Eq. (19), d and ε indicate the fiber diameter and the porosity, respectively; constants A and B are 5.55 and 10.1, respectively. For a high porosity (ε>0.7), Davis proposed the following empirical equation [57]:

$$K=d^2[64(1-\varepsilon)^{3/2}(1+56(1-\varepsilon)^3)]^{-1} \quad (20)$$

where d and ε are the fiber diameter and the porosity, respectively.

The flow inside the porous is affected by the pores structure and tortuosity. The tortuosity is calculated by the following equation [58]:

$$\tau=\frac{\Sigma\sqrt{u^2+v^2}}{\Sigma|u|} \quad (21)$$

Kaponen et al. [59] proposed the below equation to estimate tortuosity based on porosity (ε):

$$\tau=1+a\left(\frac{1-\varepsilon}{(\varepsilon-\varepsilon_c)^m}\right) \quad (22)$$

where m, a, and ε_c are 0.65, 0.19, and 0.33, respectively.

To obtain the permeability and tortuosity of the porous medium, a 3D channel with 91×91×91 nodes was considered; then, boundary conditions were applied as the pressure gradient between input and output of the fluid flow, the non-slip boundary condition for solid surfaces, Z=0 and Z=L, and the periodic boundary condition for Y=0 and Y=L. By averaging the fluid speed at the input and output planes and the use of the Darcy equation, the permeability for the porous medium produced by the presented method was obtained.

Results of the comparison between the permeability obtained from the present model and other methods are presented in Fig. 5(a). It can be seen that the results are in an acceptable accuracy.

The tortuosity of the proposed model was calculated by Eq. (21) and compared with the model presented by Koponen et al. in Fig. 5(b). The comparison of the obtained permeability and tortuosity (Fig. 5) shows that the results are logical and ensure modeling accuracy. The flow of the reactive gases at a section of the polymer fuel cell cathode (Fig. 2) was investigated in the following.

2. Simulation of Flow at Cathode

By applying the boundary conditions, assumptions and the LBM

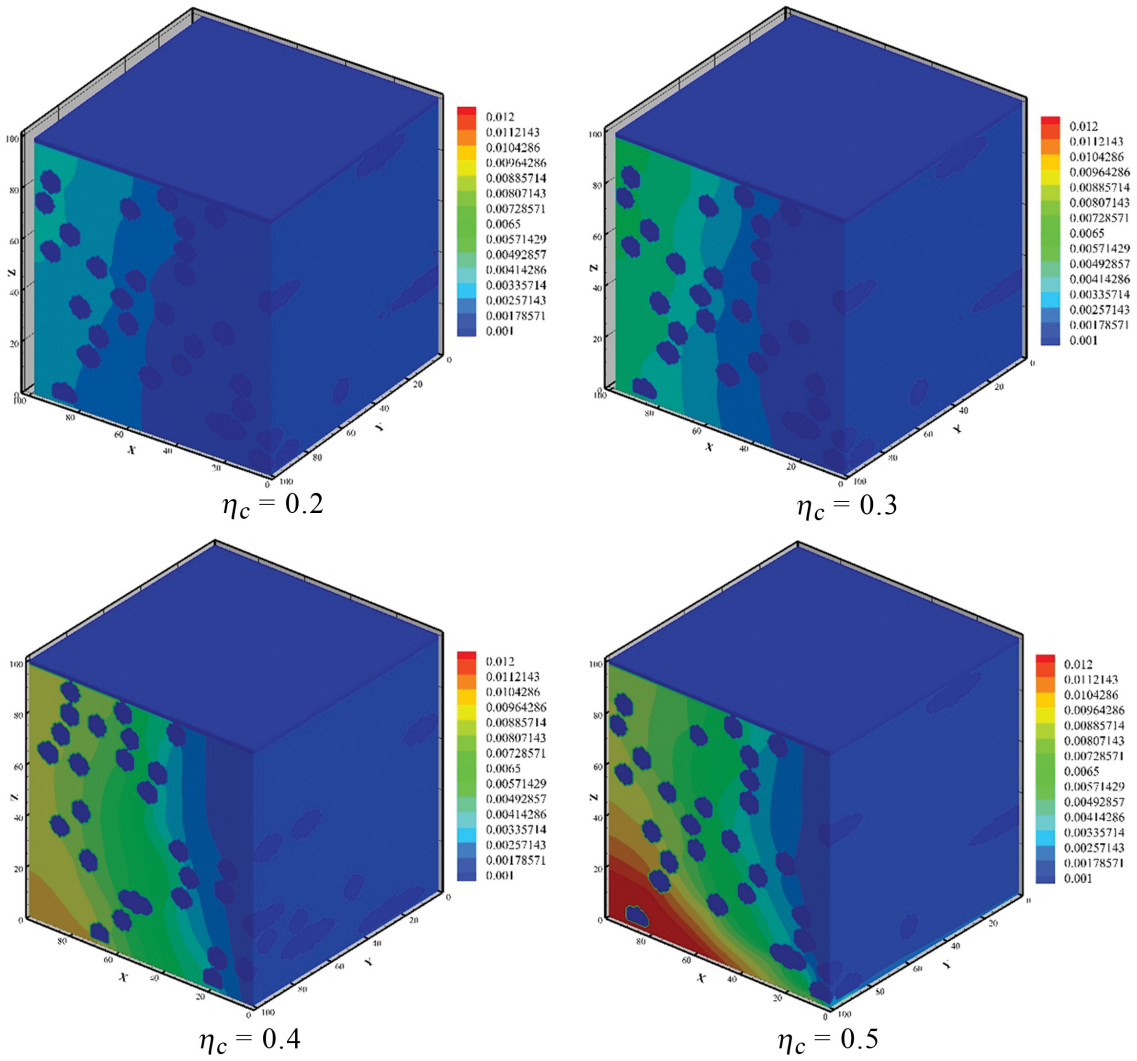

Fig. 7. Distribution of water vapor mole fraction.

active approach for an ideal gas mixture (Sec. 2), the reactant flow was investigated within the solution domain. Since the catalyst layer was considered as a reactive plane, Eqs. (10) and (13) were utilized to take into account this layer impact. Results of the reactant distribution and the electric current density with the change in the activation over-potential and the diameter of GDL carbon fiber are presented in the following.

3. Effect of Activation Potential Loss

The activation over-potential is one of the irreversibility factors of the reaction. This phenomenon is due to the low reaction rate on the electrodes; the fuel cell potential difference reduces and the current density increases by increasing this parameter. Fig. 6 shows the distribution of the oxygen density at the GDL under different over-potentials (η). According to this figure, because of the oxygen consumption on the catalyst layer, the mole fraction of oxygen reduced towards the X=L plane. The oxygen consumption increased and the oxygen density decrease in the gas diffusion layer; it is intensified by increasing the electrochemical reaction rate because of the higher activation over-potential. The molar fraction of oxygen at X=L in η=0.2, η=0.3, η=0.4, and η=0.5 was 0.199, 0.197, 0.19 and 0.18, respectively, indicating a 10% decrease in oxygen fraction in the study period. The minimal oxygen concentration appears at the X=L plane close to the catalyst as a result of the thickest diffusion layer and the smallest velocity in this region [31].

Fig. 7 shows the mole fraction of water vapor at the modeled cathode; according to this figure, the mole fraction of the water vapor in the GDL increased with the production of water, in view of the fact that the oxygen reduction occurs. The amount of produced water increased upon increasing the activation potential and reaction rate, as a result of an increase in the mole fraction of the water vapor inside the gas mixture. Moreover, the mole fraction of the water vapor around the catalyst layer gradually increased upon the increase of the activation potential; and the maximum water vapor density was seen at X=L, near the catalyst layer. The molar fraction of water vapor changes from 0.003 to 0.0165 in η=0.2 and η=0.5 values. Similar to the oxygen mole fraction profile, the water vapor mole fraction profiles are also flexuous given the porous structures of GDL.

As was said, the current density may change by many parameters, such as temperature, oxygen density, and activation over-potential. According to Eq. (11), an increase in activation potential loss has a significant effect on the current density. Fig. 8 shows the scale of this parameter effect by illustrating the distribution of the

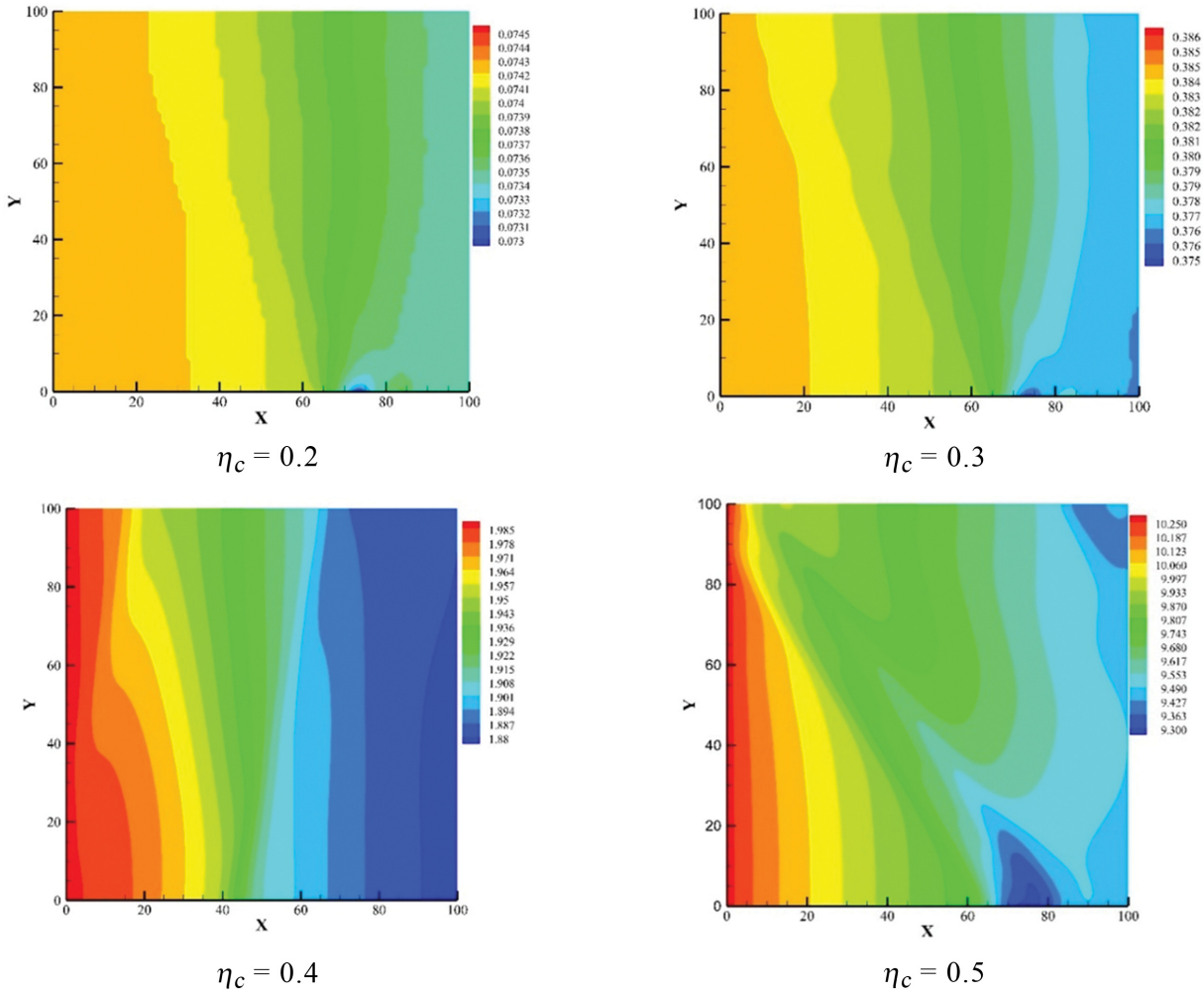

Fig. 8. Local electrical current density at catalyst layer.

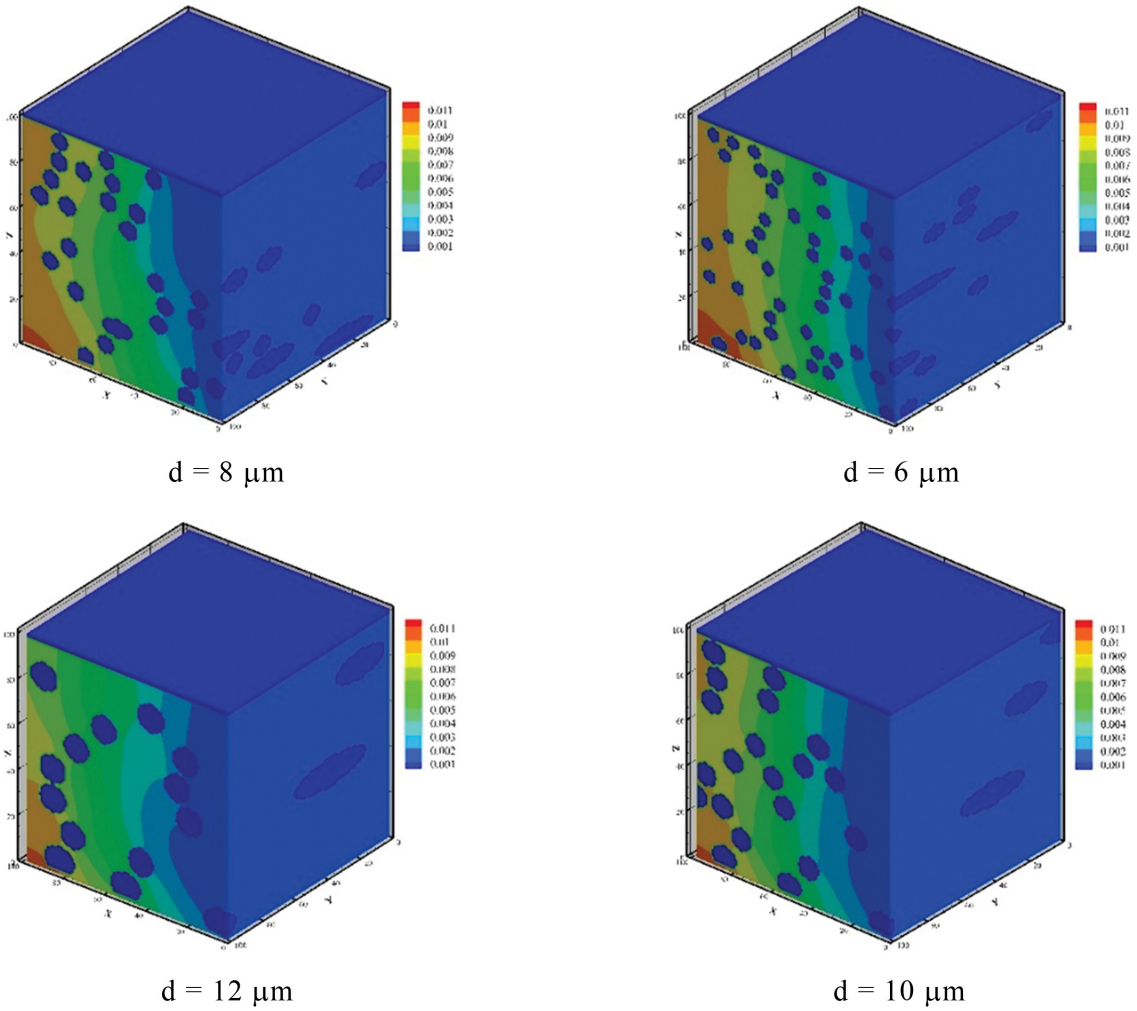

Fig. 9. Distribution of water vapor mole fraction for different fiber diameter (pore diameter).

current density over the catalyst layer. Since the oxygen reduction along the X-direction, the current density reduces along this direction and the non-homogeneous structure of the porous medium, the current distribution along the X-axis is not uniform. Due to the presence of more oxygen in the inlet air mixture, according to Eq. (11), the maximum current density will be near x=0. The maximum values of electric current at η=0.2, η=0.3, η=0.4, η=0.5 and density were 0.0743, 0.386, 1.99 and 10.2 Acm^{-2}, respectively.

According to Fig. 8, the current density increases with increasing the over-potential. Furthermore, the difference between the maximum and minimum current density increases with increasing the activation over-potential. Although the localized current density is expected to have the lowest value at X=100, due to the influence of the GDL structure on the oxygen distribution inside the cathode, the position of the minimum value of the current density is placed at the last quarter of the solution domain. For example, in η=0.3 and η=0.5 the electric current density in X=73 and X=76 is minimized.

4. Effects of the GDL Carbon Fiber Cross Section

Changes in the GDL carbon fiber diameter can alter the pores in the layer. Any change in the pores can affect the fuel cell performance by influencing the reactive gas permeability inside the GDL porous media.

To investigate how a change in diameter can affect the fuel cell performance and the distribution of reactants over the GDL, the flow of reactants and the electrochemical reaction were simulated. This simulation was performed in different carbon fiber diameters at a constant GDL porosity in the fuel cell cathode. Figs. 9 and 10 depict the mole fraction distribution of the water vapor and oxygen at the cell cathode.

Despite the fact that the oxygen flow penetrates more easily into the GDL with increasing the pore diameter (Fiber diameter), it seems that a portion of oxygen near the catalyst layer and the water vapor density at the cathode both decrease; this action may be occurring because of the enlarged pore pathway. This indicates a reduction in the electrochemical reaction, which is associated with reduced electric current and poor cell performance.

According to Figs. 9 and 10, changes in the distribution of oxygen and water vapor for large carbon fiber diameters are not considerable. In view of the fact that water vapor production and oxygen consumption reaction occur, the minimum mole fraction of oxygen and maximum mole fraction of water vapor are seen in the

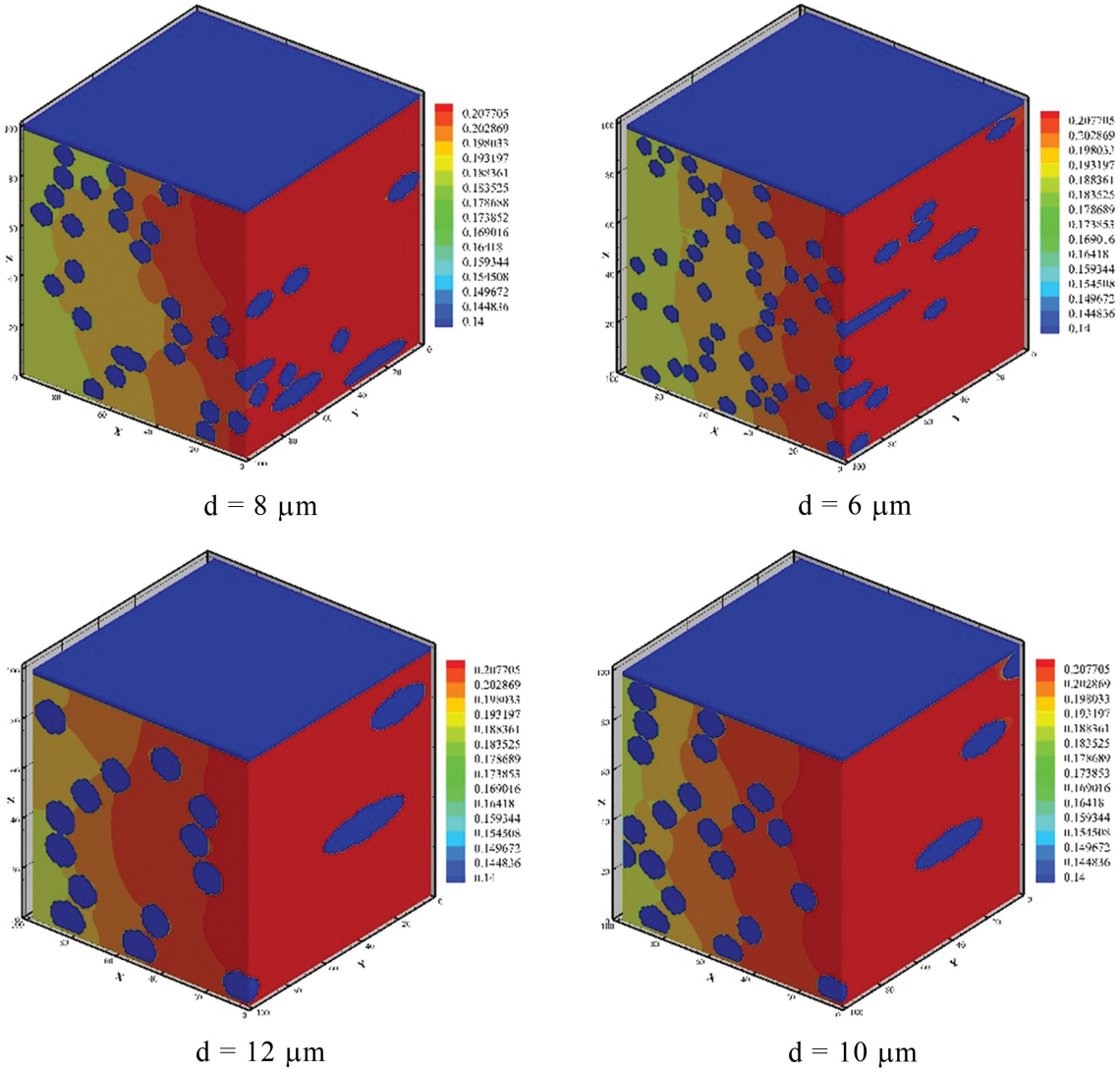

Fig. 10. Distribution of oxygen mole fraction for different fiber diameter (pore diameter).

vicinity of the catalyst layer in all cases (above 10 μm).

Fig. 11 presents the changing trend of the local current density with a change in carbon fiber diameter to provide a better understanding of the effect of carbon fiber diameter on current density produced on the bottom surface. According to these, the maximum current density was observed at the entrance of the modeled cathode (Figs. 9-10).

The oxygen mole fraction and thus the current density reduced gradually with moving towards the exit region could be attributed to the oxygen consumption and its reduction on the catalyst layer surface. From Fig. 10, lines representing the equal current density are almost along the y-direction. However, in areas where the carbon fiber is very close to the catalyst layer surface, some extent of deviation is observed, because of the oxygen inhibition. In spite the fact that the maximum and minimum current density in all cases are similar, the mean current density on the catalyst layer surface increased with increasing the diameter of the carbon fiber cross-section, although the extent of these changes is not dramatic (from 1.90 Acm^{-2} @ d=6 μm to 1.95 Acm^{-2} @ d=12 μm).

CONCLUSION

This article introduces a new and simple method based on the hardcore approach to porous medium generation. The proposed method allows the production of non-homogeneous porous media with cylindrical particles without any overlap between solid particles. This technique was applied for a 3D pore scale modeling of the fuel cell GDL. Assuming the produced water is in vapor form, the gas products exhibit ideal behavior; the flow of oxygen and water vapor species, as well as the current density, were modeled in 3D by LBM. The effects of the variation in the activation potential loss and the carbon fiber diameter on the distribution of oxygen species and water vapor were investigated. Results showed that the activation over-potential had a significant effect on the mole fraction of oxygen species and water vapor, as well as on the generated electric current. Even though the electrochemical reactions have reduced the mole fraction of output oxygen on the input surface, the water vapor generation in this reaction caused an increase in the water vapor density at the cathode. Regardless of the fact

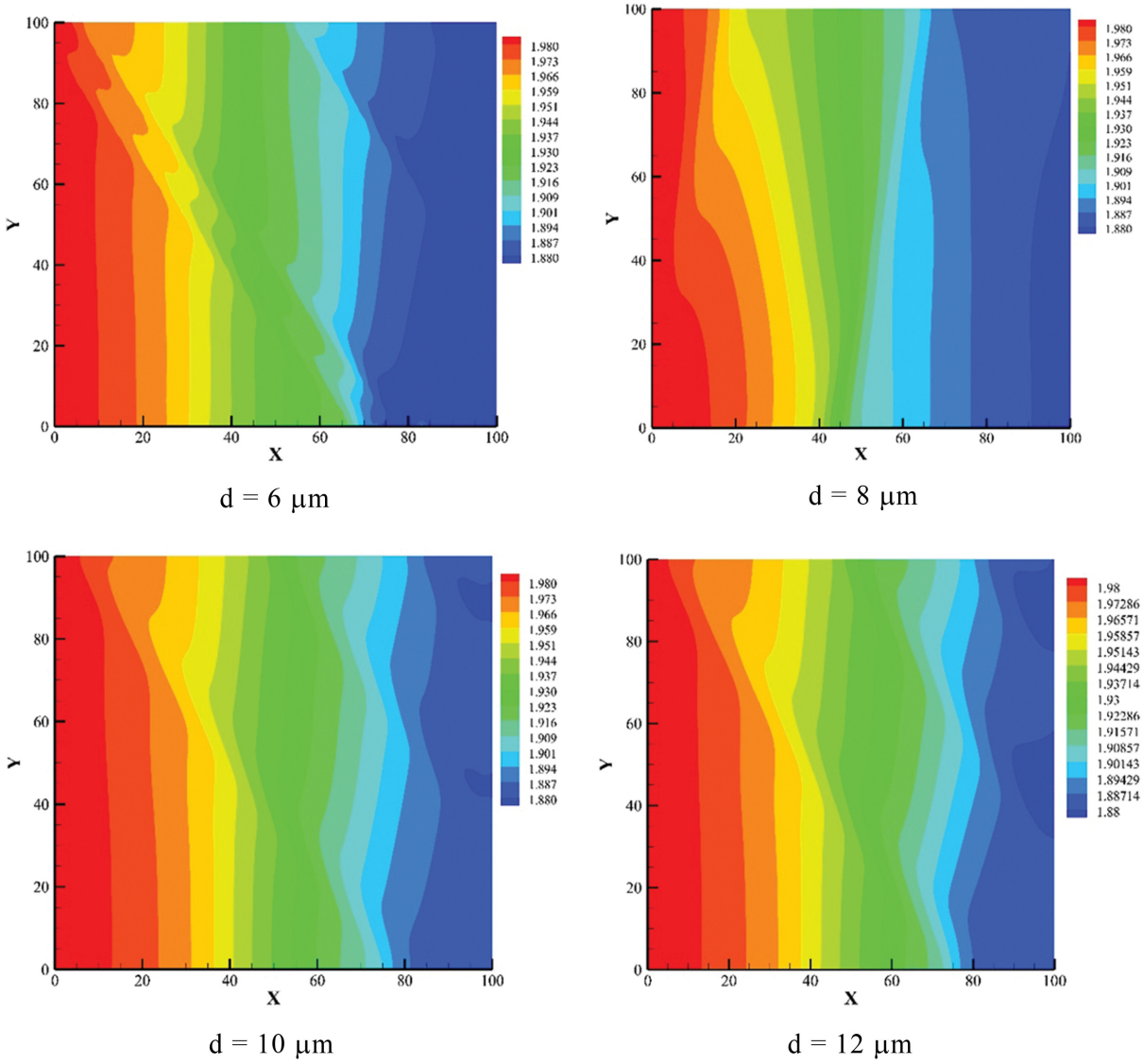

Fig. 11. Distribution of electrical current density in different fiber diameter.

that the maximum and minimum current density in all carbon fiber diameters are similar, the mean current density on the catalyst layer surface increased with increasing the diameter of the carbon fiber cross-section. Finally, the gap between the maximum and minimum of current density increased in the activation overpotential higher values.

ACKNOWLEDGEMENTS

The authors thank the reviewers and editor for the constructive comments. The authors would like to thank the Vice-chancellor for research, Shahid Chamran University of Ahvaz (Grant number: 94/3/02/315790).

REFERENCES

1. F. Barbir, *PEM fuel cells: Theory and practice*, Academic press (2012).
2. D. Feroldi and M. Basualdo, *Green Energy Technol.*, **87**, 49 (2012).
3. H. Frey and W. Münch, *BWK - Energie-Fachmagazin*, **56**, 58 (2004).
4. G. H. Song and H. Meng, *Acta Mech. Sin. Xuebao*, **29**, 318 (2013).
5. H. A. Gasteiger and M. F. Mathias, *Proc. 3rd Symp. Prot. Conduct. Membr. Fuel Cells*, 1 (2002).
6. Y. Wang, K. S. Chen, J. Mishler, S. C. Cho and X. C. Adroher, *Appl. Energy*, **88**, 981 (2011).
7. Spiegel, Colleen. PEM fuel cell modeling and simulation using MATLAB. Elsevier (2011).
8. S. Didari, T. A. L. Harris, W. Huang, S. M. Tessier and Y. Wang, *ECS Trans.*, **41**, 499 (2011).
9. J. Gostick, M. Ioannidis, M. Fowler and M. Pritzker, *J. Power Sources*, **173**, 277 (2007).
10. N. Pourmahmoud, S. Rezazadeh, I. Mirzaee and V. Heidarpoor, *J. Mech. Sci. Technol.*, **25**, 2665 (2011).
11. Z. Shi and X. Wang, *J. Fuel Cell Sci. Technol.*, **9**, 021001 (2012).
12. R. Wu, X. Zhu, Q. Liao, R. Chen and G. M. Cui, *Int. J. Hydrogen Energy*, **38**, 4067 (2013).

13. Y. Lee, *J. Mech. Sci. Technol.*, **31**, 1959 (2017).
14. M. Abdollahzadeh, J. C. Pascoa, A. A. Ranjbar and Q. Esmaili, *Energy*, **68**, 478 (2014).
15. N. H. Maslan, M. M. Gau, M. S. Masdar, and M. I. Rosli, *J. Eng. Sci. Technol.*, **11**, 85 (2016).
16. M. Liang, Y. Liu, B. Xiao, S. Yang, Z. Wang and H. Han, *Int. J. Hydrogen Energy*, **43**, 17880 (2018).
17. Y. Wang, C. Y. Wang and K. S. Chen, *Electrochim. Acta*, **52**, 3965 (2007).
18. V. Radhakrishnan and P. Haridoss, *Mater. Des.*, **32**, 861 (2011).
19. K.-J. Lee, J. H. Nam and C.-J. Kim, *Electrochim. Acta*, **54**, 1166 (2009).
20. H. Ostadi, P. Rama, Y. Liu, R. Chen, X. X. Zhang and K. Jiang, *Chem. Eng. Sci.*, **65**, 2213 (2010).
21. J. Becker, V. Schulz and A. Wiegmann, *J. Fuel Cell Sci. Technol.*, **5**, 021006 (2008).
22. L. Vázquez, A. H. Creus, P. Carro, P. Ocón, P. Herrasti, C. Palacio, J. M. Vara, R. C. Salvarezza and A. J. Arvia, *J. Phys. Chem.*, **96**, 10454 (1992).
23. M. Göbel, M. Godehardt and K. Schladitz, *J. Power Sources*, **355**, 8 (2017).
24. J. Liao, G. Yang, S. Li, Q. Shen, Z. Jiang, H. Wang, L. Xu, M. Espinoza-Andaluz and X. Pan, *Energy Fuels*, **35**(3), 2654 (2021).
25. A. H. Kakaee, G. R. Molaeimanesh and M. H. Elyasi Garmaroudi, *Int. J. Hydrogen Energy*, **43**, 15481 (2018).
26. Y. T. Mu, L. Chen, Y. L. He and W. Q. Tao, *Build. Environ.*, **92**, 236 (2015).
27. R. Bahoosh, M. Jafari and S. S. Bahrainian, *J. Heat Mass Transf. Res.*, **6**, 105 (2019).
28. L. Chapelle, M. Lévesque, P. Brøndsted, M. R. Foldschack and Y. Kusano, in *ICCM Int. Conf. Compos. Mater.* (2015).
29. K. Schladitz, S. Peters, D. Reinel-Bitzer, A. Wiegmann and J. Ohser, *Comput. Mater. Sci.*, **38**, 56 (2006).
30. C. Peyrega, D. Jeulin, C. Delisée and J. Malvestio, *Image Anal. Stereol.*, **28**, 129 (2009).
31. L. Chen, H.-B. Luan, Y.-L. He and W.-Q. Tao, *Int. J. Therm. Sci.*, **51**, 132 (2012).
32. V. P. Schulz, J. Becker, A. Wiegmann, P. P. Mukherjee and C.-Y. Wang, *J. Electrochem. Soc.*, **154**, B419 (2007).
33. L. Hao and P. Cheng, *J. Power Sources*, **186**, 104 (2009).
34. Y. Wang, S. Cho, R. Thiedmann, V. Schmidt, W. Lehnert and X. Feng, *Int. J. Heat Mass Transf.*, **53**, 1128 (2010).
35. J. Feder, *J. Theor. Biol.*, **87**, 237 (1980).
36. F. Naddeo, N. Cappetti and A. Naddeo, *Comput. Mater. Sci.*, **81**, 239 (2014).
37. H. Moussaddy, *Doctoral dissertation*, Montral University (2013).
38. N. Provatas, M. Haataja, J. Asikainen, S. Majaniemi, M. Alava and T. Ala-Nissila, *Colloids Surfaces A Physicochem. Eng. Asp.*, **165**, 209 (2000).
39. G. Falcucci, S. Ubertini, E. Galloni and E. Jannelli, in *EFC 2009 - Piero Lunghi Conf. Proc. 3rd Eur. Fuel Cell Technol. Appl. Conf.* (2009).
40. B. Han, J. Yu and H. Meng, *J. Power Sources*, **202**, 175 (2012).
41. L. Xiao, M. Luo, H. Zhang, R. Zeis and P.-C. Sui, *J. Electrochem. Soc.*, **166**, F377 (2019).
42. G. R. Molaeimanesh, M. H. Shojaeefard and M. R. Moqaddari, *Korean J. Chem. Eng.*, **36**, 136 (2019).
43. P. L. Bhatnagar, E. P. Gross and M. Krook, *Phys. Rev.*, **94**, 511 (1954).
44. G. R. Molaeimanesh and M. H. Akbari, *Korean J. Chem. Eng.*, **32**, 397 (2015).
45. X. Shan and H. Chen, *Phys. Rev. E*, **47**, 1815 (1993).
46. A. A. Mohamad, *Lattice boltzmann method, 2nd Ed.*, Springer-Verlag, London (2011).
47. S. Succi, Oxford Univ. Press, Oxford (2001).
48. H. R. Ashorynejad, K. Javaherdeh and H. E. A. Van den Akker, *Int. J. Hydrogen Energy*, **41**, 14239 (2016).
49. M. R. Kamali, S. Sundaresan, H. E. A. Van den Akker and J. J. J. Gillissen, *Chem. Eng. J.*, **207**-**208**, 587 (2012).
50. L. Vinet and A. Zhedanov, *Arch. Ophthalmol.*, **122**, 552 (2010).
51. H. Anton, *Methods Enzymol.*, **461**, 397 (2009).
52. G. R. Molaeimanesh and M. H. Akbari, *J. Power Sources*, **258**, 89 (2014).
53. Q. Zou and X. He, *Phys. Fluids*, **9**, 1591 (1997).
54. D. A. Nield and A. Bejan, *Convection in porous media*, Springer, New York (2013).
55. M. Kaviany, *Mech. Eng. Ser.*, **53**, 726 (1995).
56. A. Koponen, D. Kandhai, E. Hellén, M. Alava, A. Hoekstra, M. Kataja, K. Niskanen, P. Sloot and J. Timonen, *Phys. Rev. Lett.*, **80**, 716 (1998).
57. C. N. Davies, *Proc. Inst. Mech. Eng.*, **167**, 185 (1952).
58. O. Filippova and D. Hänel, *J. Comput. Phys.*, **147**, 219 (1998).
59. A. Koponen, M. Kataja and J. Timonen, *Phys. Rev. E - Stat. Physics, Plasmas, Fluids, Relat. Interdiscip. Top.*, **56**, 3319 (1997).